Interfacial wave dynamics of a drop with an embedded bubble

S. Bhattacharya

Interfacial wave dynamics of a drop with an embedded bubble

S. Bhattacharya[1]

[1]*Department of Mechanical Engineering, Texas Tech University, Lubbock, Texas 79409, USA*

This article describes how an embedded bubble changes the surface wave of a suspended liquid drop, and how such modifications, if recorded experimentally, can be used to detect voids in typically opaque interior of the fluid. The analysis uses a matrix formalism to predict the frequencies for natural oscillation and the deformation for acoustically induced forced vibration. The theory shows that the embedded cavity causes major shifts in the frequency and amplitude values as well as twofold increase in number of natural modes indicating multi-facetted utility of the results in process diagnostics, material characterizations and combustion technology.

I. INTRODUCTION

Wave dynamics at the surface of a drop first studied by Lord Rayleigh [1] has been a popular topic in physics due to its relevance in fields ranging from stellar dynamics [2] to nuclear collision [3]. Interestingly, presence of a bubble inside the droplet causes major changes in its interfacial oscillation not only by altering frequencies and amplitudes of vibration but also by introducing entirely new natural modes. Our analysis describes such phenomena by predicting natural frequencies, deformed shapes and resonance features of the bubble-drop system undergoing either free or sonically induced forced vibration.

Surprisingly, these important effects have never been mathematically analyzed despite century-long research [4–9] on this subject. For example, many past papers have described dynamics of compound drops where one medium is surrounded by another. Such works either investigated vibration of thin liquid shells [10, 11], or used numerical simulations to compute temporal evolution of interfaces with axisymmetric perturbation [12, 13], or approximated flow solutions to infer on stability features [14]. None of these, however, produced exact mathematical results for natural frequencies of the two-phase droplet assuming appropriate physical conditions.

Advent of high-speed camera as well as new scopes in combustion and manufacturing technologies assure multi-facetted impact of the aforementioned findings on several branches of contemporary science. Changes in interfacial oscillation recorded by an optical device can be exploited to detect bubbles or solid particles in typically opaque interior of a drop. Such ability is especially useful for understanding and improving novel combustive and manufacturing systems. For example, our recent high-speed imaging [15] described dynamics of spark-ignited nano Aluminum in an unpublished work. The observation reveals initial detachment, subsequent pulsation, occasional fragmentation and eventual explosion of metallic droplets. There, an anomalous pulsation frequency indicated presence of gas filled cavities in the detached liquid leading to proper explanation of the entire process where the gaseous voids promote internal oxidation and excess deformation causing the final explosive display. In-depth study of surface wave in bubble- or particle-laden drop can provide similar crucial insights into spraying techniques [16], particle depositions [17], fuel combustion [18], and material processing [19].

Added utility of our theory comes from its ability to describe resonance characteristics of a bubble-laden drop forced to vibrate in an acoustic field. If proper resonance occurs, sound waves can facilitate fragmentation of droplets [20]. In a combustive environment, such phenomenon can cause orders of magnitude increase in burn rate leading to significantly enhanced efficiency and explosive power [21]. Moreover, better understanding of acoustic interactions with an interface may lead to a new sonoluminescent system [22] in mesoscopic drops where the small size enhances the role of capillary effect typically absent in macroscopic bulk. The resultant hot spots created by ultrasonic excitation can be used as a self-ignition mechanism for liquid fuels. Also, the introduced matrix formulation can be generalized for solid bodies so that their interior defects [23] can be conveniently revealed by forced vibration at their surface. Similarly, it can be used to explain vibrational dynamics of foams which remained the topic of interest in many past and contemporary studies [24, 25].

This paper is organized in the following way. In section II, we outline the flow-analysis for free oscillation of a bubble-laden drop where a quantum mechanical matrix formalism predicts the natural frequencies. The corresponding interfacial configurations for Eigen modes are illustrated in section III. Then, the deformation amplitude and the resonance characteristics for acoustically induced forced vibration of the droplet are described in section IV. Finally, the article is concluded in section V explaining how the findings can be used for in-vivo diagnostics and other technological purposes.

II. NATURAL MODES FOR INTERFACIAL WAVES

In our analysis, a bubble of radius a_1 resides inside a drop of radius a_0 where density of the surrounding atmosphere and the gas trapped in the cavity is approximated to be very small. The viscosity, density and surface tension coefficient of the liquid are denoted by μ, ρ and γ, respectively. Our first goal is to express the natural frequencies of the surface wave as functions of the
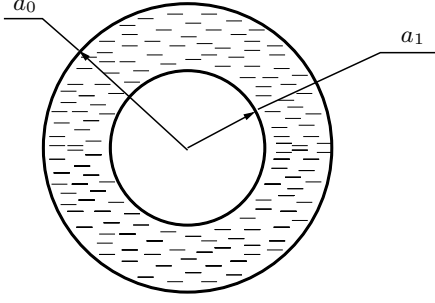
FIG. 1: Schematic picture for the unperturbed drop with embedded bubble.

size-ratio $\tilde{a} = a_1/a_0$ so that the influence of the cavity on interfacial dynamics can be quantified. To highlight the desired effect in the simplest way, a spherically symmetric geometry of the unperturbed system is assumed. The theory can be generalized in the future for an eccentrically placed void in the liquid by using appropriate transformations [27–30] between flow solutions centered around the respective misaligned spheres. For this article, however, the undeformed liquid domain is confined between two concentric interfaces as shown in Fig.1.

The characteristic amplitude A_s for the deformation at the boundary of the liquid domain is considered to be small compared to a_0. The corresponding velocity-scale is given by $A_s\sqrt{\gamma/(\rho a_0^3)}$ for which the ratio between convective and temporal accelerations becomes A_s/a_0 — a small quantity compared to unity. Hence, flow equations remain linear due to insignificant contribution from convective inertia. For such systems, the ratio of viscous and interfacial forces is given by capillary number Ca which is $\mu A_s/\sqrt{\gamma\rho a_0^3}$. Similarly, the Bond number $B_o = g\rho a_0^2/\gamma$ represents the relative importance of gravity g compared to surface tension. For milimeter size water droplets, Bo is around 0.1 whereas Ca becomes of similar order when A_s/a_0 is less than 0.1. For metallic liquids, these values are even lower. Our analysis presumes the dimensional parameters to be such that both Ca and Bo are small. As a result, effects of viscous dissipation and gravity are neglected in the formulation as long as $\tilde{a}$ does not approach to 0 or 1. For $\tilde{a}\to 0$, the dynamics is dictated by an additional dimension in the form of a_1 beside the usual scale a_0, where a second capillary number with a_0 replaced by a_1 in Ca is also relevant. Similarly, when $\tilde{a} \to 1$, the thickness of the liquid shell $(a_0 - a_1)$ plays a crucial role with effective Ca modified to $A_s\sqrt{\gamma/[\rho a_0^2(a_0 - a_1)]}$. In such limiting cases, viscous dissipation can be neglected only if all involved capillary numbers are small.

If the capillary and Bond numbers are small, the following momentum and continuity equations corresponding to an incompressible liquid relate pressure (p) and displacement (**s**) fields:

$$\rho\frac{\partial^2 \mathbf{s}}{\partial t^2} = -\nabla p \qquad \text{and} \qquad \nabla^2 p = 0, \qquad (1)$$

where t is time. If viscous effect is small, boundary conditions at two free surfaces become

$$@\; r = a_i \qquad p = -\gamma[2\mathbf{s}\cdot\mathbf{n}_i/a_i^2 + \nabla_s^2(\mathbf{s}\cdot\mathbf{n}_i)]. \qquad (2)$$

Here, the subscript i can be 0 or 1 so that interfaces are defined when radial coordinate r is a_0 or a_1. The unit normal vector pointing away from the liquid domain at the i-th surface is $\mathbf{n}_i$, whereas ∇_s represents gradient on a spherical surface.

The fields p and $\mathbf{s}$ are solved as expansions of spherical harmonics $Y_{lm}(\theta, \phi)$ in angular coordinates θ and ϕ:

$$p = \rho\sum_{lm}\left[Y_{lm}\left\{(r/a_0)^l\ddot{\alpha}_{lm}^+ + (a_0/r)^{l+1}\ddot{\alpha}_{lm}^-\right\}\right], \qquad (3)$$

and

$$\mathbf{s} = -\nabla\sum_{lm}\left[Y_{lm}\left\{(r/a_0)^l\alpha_{lm}^+ + (a_0/r)^{l+1}\alpha_{lm}^-\right\}\right]. \qquad (4)$$

In eqs.3 and 4, dot denotes time derivatives while unknown unsteady amplitudes of regular and singular harmonics with indices l and m are $\alpha_{lm}^+(t)$ and $\alpha_{lm}^-(t)$. The index l can be any natural number like $1, 2, 3\ldots$, whereas m takes integer values varying from $-l$ to l.

For spherically symmetric unperturbed geometries, terms with different indices l and m are not coupled due to the separable form of the solutions. Moreover, for such configuration, the dynamic equation for a harmonic mode remains invariant of m, as neither eqs.1 and 2 nor the radial variation in fields involve m explicitly. These facts assure that if eqs.1 and 2 are converted to a matrix form, it will be block diagonal in l and degenerative in m. Thus, modes can be first analyzed for individual l, and then superposed to describe the surface wave. Accordingly, pressure and radial displacement at two interfaces induced by a specific harmonic mode Y_{lm} can be expressed by time-dependent Dirac's vectors $|p_{lm}\rangle$ and $|s_{lm}\rangle$ with two components being respective amplitudes at $r = a_0$ and $r = a_1$. We also consider another column $|\alpha_{lm}\rangle$ which is $\{\alpha_{lm}^+ \; \alpha_{lm}^-\}^{\mathrm{T}}$. The natural frequency for the dynamic phenomenon can be obtained from the matrix relations among $|p_{lm}\rangle$, $|s_{lm}\rangle$ and $|\alpha_{lm}\rangle$.

Three matrix operators relate $|p_{lm}\rangle$, $|s_{lm}\rangle$ and $|\alpha_{lm}\rangle$ to each other. Firstly, if eq.2 is expanded in spherical harmonics, equality between expansion terms at both sides of the equation ensures $|p_{lm}\rangle = (\gamma/a_0^2)(l^2 + l - 2)\hat{\mathsf{B}}|s_{lm}\rangle$. Here, the l-dependent scalar prefactor appears as the eigen value of the operator $(-2 - a_i^2\nabla_s^2)$ acting on its eigen function Y_{lm}. The diagonal matrix $\hat{\mathsf{B}}$ distinguishes the difference in radii at the outer and inner spheres

$$\hat{\mathsf{B}} = \begin{bmatrix} 1 & 0 \\ 0 & -\tilde{a}^{-2} \end{bmatrix}. \qquad (5)$$

Moreover, if r is replaced by a_0 or a_1 in eqs.3 and 4, the expansion of pressure and radial displacement at the interfaces can be obtained. The resulting expressions from the individual terms are, then, recast into two additional equalities: $|p_{lm}\rangle = \rho\hat{\mathsf{F}}_l|\ddot{\alpha}_{lm}\rangle$ and $|s_{lm}\rangle = -(1/a_0)\hat{\mathsf{H}}_l|\alpha_{lm}\rangle$ where the coupling coefficients are given by

$$\hat{\mathsf{F}}_l = \begin{bmatrix} 1 & 1 \\ \tilde{a}^l & \tilde{a}^{-l-1} \end{bmatrix} \qquad \hat{\mathsf{H}}_l = \begin{bmatrix} l & -(l+1) \\ l\tilde{a}^{l-1} & -(l+1)\tilde{a}^{-l-2} \end{bmatrix}. \qquad (6)$$

We use the relations involving $\hat{\mathsf{B}}$ and $\hat{\mathsf{H}}_l$ to substitute $|p_{lm}\rangle$ and $|\alpha_{lm}\rangle$ in terms of $|s_{lm}\rangle$ in matrix equation with $\hat{\mathsf{F}}_l$. Then rearranging one finds

$$|\ddot{s}_{lm}\rangle = -(l^2 + l - 2)\frac{\gamma}{\rho a_0^3}\hat{\mathsf{M}}_l|s_{lm}\rangle, \qquad (7)$$

where $\hat{\mathsf{M}}_l = \hat{\mathsf{H}}_l\hat{\mathsf{F}}_l^{-1}\hat{\mathsf{B}}$ is a symmetric matrix — an expected artifact due to Sturm-Liouville symmetry of eq.1. For $l \geq 1$, it remains positive definite making the dynamics restorative corresponding to an oscillatory phenomenon.

It is to be noted that the factor (l^2+l-2) in eq.7 makes $|\ddot{s}_{lm}\rangle = 0$ in eq.7 for $l=1$. This happens because harmonic modes with $l=1$ only induce translation, not surface deformations. There can be two such perturbations — 1) an overall displacement of the entire body, or 2) a relative off-centering of the cavity with respect to the liquid mass. The former induces a neutral stability for all conditions. In contrast, the latter can exhibit gradual departure from the concentric configuration depending on the initial relative velocity between two spherical interfaces. In absence of any viscous effect, the system would tend to maintain the same relative velocity as long as the bubble is not far away from the center of the drop. However, when the relative position becomes highly eccentric, it is not easy to predict whether the void would accelerate, or it would slow down to an intermediate equilibrium configuration. Our future work on the generalized geometry will explain this phenomenon precisely.

When l is natural numbers like $1, 2, 3, \ldots$, the interfacial deformation ensures fixed volumes for both the drop and the bubble. In contrast, if $l=0$, eq.7 represents a volumetric change in the domain. In that case, the matrix $\hat{\mathsf{M}}_l$ becomes negative definite indicating an unphysical situation where either the bubble disappears or the outer surface explodes to infinity over time. Such unrealistic behavior is understandable, because fluctuation in volume is dependent on consideration of thermodynamic states which is not accounted for in the present analysis.

For $l > 0$, both Eigen values $\lambda_l^\pm$ of $\hat{\mathsf{M}}_l$ (referred as plus and minus spectral modes from now on) are related to the natural frequencies $\omega_l^\pm$ implying existence of two such values for each l. In absence of a void inside, each l yields only one frequency indicating a twofold increase in number of natural modes for bubble-laden drop. Figure 2 presents normalized $\omega_l^\pm$ for $l=2, 3$ as functions of $\tilde{a}$.

We define $\tilde{\omega}_l^\pm = \omega_l^\pm/\sqrt{\gamma/(\rho a_0^3)} = \sqrt{(l^2+l-2)\lambda_l^\pm}$ to represent dimensionless frequency. Then, we find asymptotic expressions $\tilde{\omega}_l^{a+} = \sqrt{(l+2)(l^2-1)/[\tilde{a}^3 - \tilde{a}^{(l+7)/2}]}$ and $\tilde{\omega}_l^{a-} = \sqrt{(l^3+l^2-2l)[1-\tilde{a}^{(l+1)/2}]}$ for both $\tilde{\omega}_l^\pm$ by exploiting the exact forms of $\hat{\mathsf{B}}$, $\hat{\mathsf{F}}_l$ and $\hat{\mathsf{H}}_l$. These limiting results are constructed in such a way that $\tilde{\omega}_l^{a\pm}$ become the frequencies simultaneously for two cases $\tilde{a} \to 0$ and $\tilde{a} \to 1$. Such dual validity is achieved by including two terms with two different exponents of $\tilde{a}$ in the relations describing $\tilde{\omega}_l^{a\pm}$. As a result, it is seen that the plus mode varies as a_l^{-3} for diminishing bubble size and as $(a_0 - a_1)^{-1}$ for thin liquid shell. In contrast, the minus mode would be always dictated by the nominal length-scale a_0.

The ratios of $\tilde{\omega}_l^\pm$ and corresponding asymptotic values are plotted in Fig.2 for $0 \leq \tilde{a} \leq 1$ where the curves converge to 1 at both ends. Rayleigh's classical analysis
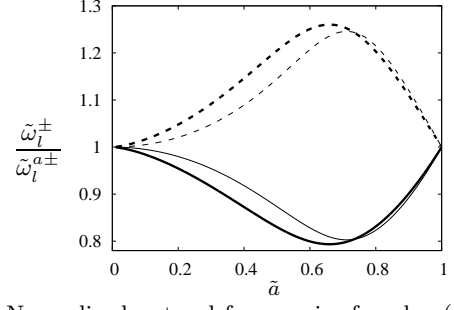

FIG. 2: Normalized natural frequencies for plus (solid lines) and minus (dashed lines) spectral modes are plotted as functions of size-ratio when $l=2$ (thick lines) and $l=3$ (thin lines).

predicts $\tilde{\omega}_l^{a-}$ with $\tilde{a} \to 0$ to be the natural frequency of a continuous drop. Our results for $\tilde{\omega}_l^-$ show how the finite size of the bubble modifies it. Moreover, the additional mode $\tilde{\omega}_l^+$ scales approximately as inverse square-root of the volume fraction of the cavity, and causes extra complexity in the dynamics.

III. SURFACE CONTOURS FOR EIGEN MODES

Study of interfacial shapes formed in representative natural modes can explain the dynamics better. This needs computing deformations at $r = a_0$ and $r = a_1$ for certain l and Eigen vectors of $\hat{\mathsf{M}}_l$. As $\hat{\mathsf{M}}_l$ is a symmetric operator, its Eigen vectors $|e_l^\pm\rangle$ associated to Eigen values $\lambda_l^\pm$ are orthogonal implying $|e_l^\pm\rangle = \{\pm\eta_l^{\pm 1}\ 1\}^T$, where η_l is a parameter dependent on $\tilde{a}$ and l. Construction of surface contours requires η_l as it shows relative radial perturbations at the droplet and the embedded bubble.

In Fig.3, we present η_l as function of $\tilde{a}$ for $l=2, 3$. For $\tilde{a} \to 0$, the limiting value of η_l is $\eta_l^a = (2l+1)\tilde{a}^{l+2}/(l+1)$. A ratio of η_l and η_l^a is plotted in Fig.3 so that all curves start at a value 1 for $\tilde{a}=0$. As a result, one can construct Eigen vectors $|e_l^\pm\rangle$ for any geometry. Thus, we can find how much the outer surface of the drop would deform for given perturbation at the bubble surface if the harmonic and spectral modes are specified.

In Figs.4 and 5, we present two intrinsically different classes of interfacial configurations of a bubble-laden drop with volume fraction of the void being 0.3 — a nearly typical value expected in combustion of porous solid fuels like nano Aluminum. In both figures, we present inter-
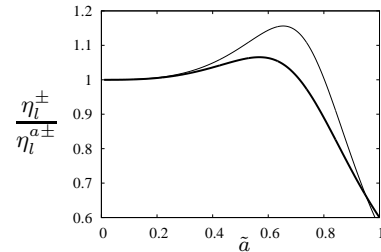

FIG. 3: Normalized component ratio vs. size-ratio for $l=2$ (thick line) and $l=3$ (thin line).
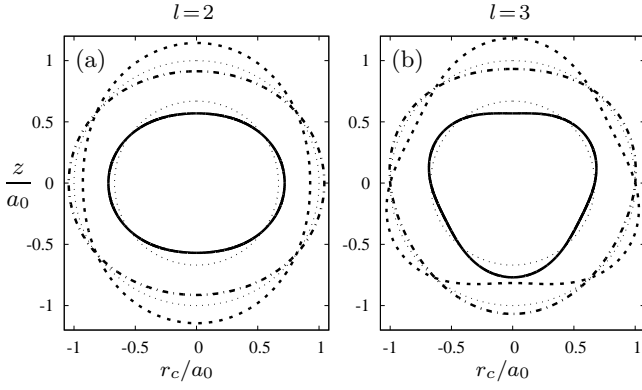
FIG. 4: Longitudinal section of the axisymmetric interfacial shape with $m=0$ and $l=2$ (Fig.4a at left) or $l=3$ (Fig.4b at right). The outer surface of the deformed drop is described for plus (dash-dot lines) and minus (dashed lines) spectral modes with given perturbation of the deformed bubble (solid lines). The faint dotted lines represent both unperturbed interfaces.

FIG. 5: Vertical x-z (top row with Figs.5a,b) and horizontal x-y (bottom row with Figs.5c,d) sections of the interfaces with $m=\pm l$ and $l=2$ (left panel with Figs.5a,c) or $l=3$ (right panel with Figs.5b,d). The configurations for the droplet and the bubble surfaces are denoted by the similar line types as in Fig.3.

facial configurations for $l=2,3$ as well as for plus and minus spectral modes. However, the difference between Figs.4 and 5 is in the geometric symmetries. The first one describes axisymmetric cases with $m=0$, where the shape can be observed in any longitudinal section defined by cylindrical radius r_c and axial coordinate z. In contrast, Fig.5 shows the modes with $m=\pm l$, where the fields have only x-y variation, though the contours of initially spherical interfaces would require two sectional views for visualization. Hence Fig.5 includes both x-y and x-z views for complete depiction of the systems.

For $l=2$, an initially spherical geometry deforms to an approximate ellipse. For $l=3$, in contrast, the final contours become triplon-like structures [26]. In both cases, the relative orientation of deformations at inner and outer surfaces would be different for plus and minus spectral modes because of the orthogonality between Eigen vectors $|e_l^{\pm}\rangle$.

To highlight the distinction between the plus and minus modes, Figs.4 and 5 ensure the inner bubble has exact same perturbation for both spectral modes. For example, when $l=2$, the deformed void is always represented by an ellipse with horizontal major axis along the x-axis. Then, the external interface of the droplet also deforms to ellipsoidal shape, but its orientation differs for $|e_2^-\rangle$ and $|e_2^+\rangle$. In case of the minus mode, the major axis for the outer periphery becomes vertical, so that the engulfing drop and the embedded bubble become perpendicularly placed. In contrast, for $|e_2^+\rangle$, two interfaces reach to perfect alignment with both of their elongated dimension coinciding along the x-axis. Additionally, the amount of eccentricity at the exterior is more for $|e_2^-\rangle$ compared to $|e_2^+\rangle$. Similar distinction can be observed for triplon contours with $l=3$ also. This means the lower frequency nearer to the Rayleigh's prediction happens when two interfaces are not aligned, whereas the extra higher value appears when the configurations are in sync. It can be concluded that the former can instigate disintegration of
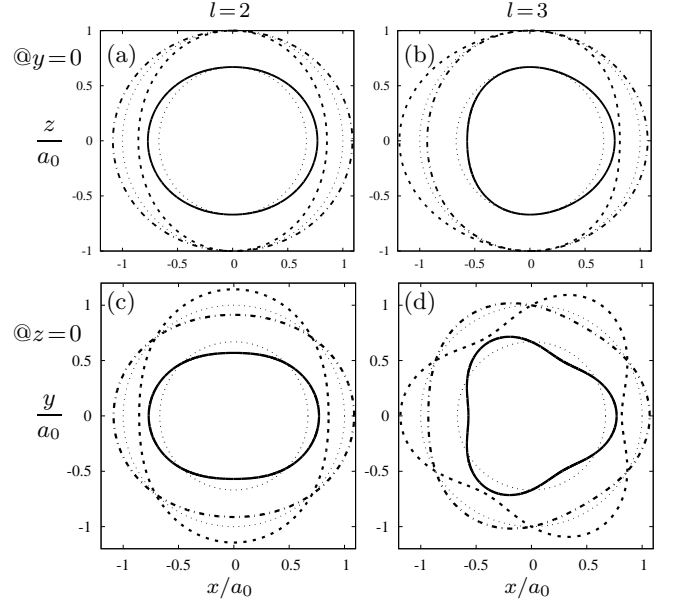
the drop quicker, as the misaligned more deformed bubble approaches closer to the outer periphery.

IV. FORCED VIBRATION OF THE DROPLET

Acoustically induced forced vibration of a bubble-laden drop can be analyzed by introducing a forcing term in eq.7. If a pressure wave with frequency Ω excites the outer surface of the drop, one has to modify eq.2 for $i=0$. Consequently, eq.7 alters to the following form:

$$|\ddot{s}_{lm}\rangle + \frac{(l^2+l-2)}{\rho a_0^3/\gamma}\hat{\mathsf{M}}_l|s_{lm}\rangle = \frac{p_{lm}^{\mathrm{ex}}}{\rho a_0}\hat{\mathsf{H}}_l\hat{\mathsf{F}}_l^{-1}|i^{\mathrm{ex}}\rangle\sin(\Omega t). \quad (8)$$

Here $|i^{\mathrm{ex}}\rangle = \{1\ \ 0\}^T$ is a unit vector indicating only contribution at the external interface, and p_{lm}^{ex} is the amplitude of the pressure wave expanded in Y_{lm} at $r=a_0$. In real situation, any arbitrary pressure fluctuation would involve a number of modes with different l and m superposed to represent the actual spatial variation of the field. Our analysis would be applicable to each of these individual modes.

Solution of eq.8 is $|s_{lm}\rangle = (p_{lm}^{\mathrm{ex}}a_0^2/\gamma)\sin(\Omega t)|\zeta_l\rangle$ where $|\zeta_l\rangle = \hat{\mathsf{N}}_l|i^{\mathrm{ex}}\rangle$ and $\hat{\mathsf{N}}_l = [(l^2+l-2)\hat{\mathsf{B}}-\tilde{\Omega}^2\hat{\mathsf{F}}_l\hat{\mathsf{H}}_l^{-1}]^{-1}$ with $\tilde{\Omega}$ being dimension-less forcing frequency $\Omega/\sqrt{\gamma/(\rho a_0^3)}$. The drop vibration by acoustic excitation can be characterized by the ratio of deformation to pressure amplitudes. This quantity given by $(a_0^2/\gamma)|\zeta_l\rangle$ is termed as mode deformability which is normalized by a_0^2/γ and represented by $|\zeta_l\rangle$ in non-dimensional form. Its first and second components quantify deformations at the outer and inner interfaces per unit harmonic amplitude of forcing pressure field. These are referred as ζ_l^{ex} and ζ_l^{in}, respectively.
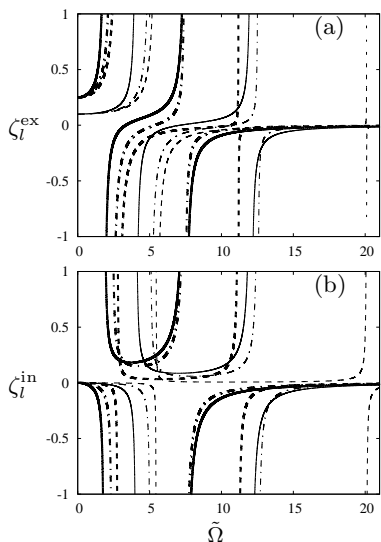
$$C_\nu(\omega) = \int s^{\text{ex}}(t,\beta)\, e^{i\nu\beta} e^{i\omega t} d\beta\, dt. \qquad (9)$$

Complete spectral description of the dynamics requires C_ν to be evaluated as function of ω for $\nu = 0,1$. Consequently, spectral plots of C_ν in frequency domain will show several spikes, where all natural frequencies for even and odd l's would be revealed by C_0 and C_1, respectively. These values can be used to predict the size of the cavity inside the drop by matching the observation with the theoretical predictions.

We also describe the interfacial contours for the natural modes to illustrate the relative deformation of the embedded bubble and the engulfing drop. These results can be coupled with the resonance features seen in the analysis of forced vibration to manipulate acoustically accelerated break-up of droplets. Such inference can be drawn from a linear stability analysis in presence of viscous effects. Then one can conclude whether the resonating system would stabilize or diverge to an unstable state. We plan to address this problem in the near future.

The matrix formulation can be generalized for viscous systems where decay characteristics of amplitudes are expected along with the oscillatory behavior. Also one can modify the theory for an embedded particle instead of a bubble inside the drop. Such alterations would significantly increase the scope of the presented analysis.

The theory can be extended to many-bubble or many-particle systems inside a drop. This needs use of recently developed basis transformation method [27–30] to enforce boundary conditions at disconnected dissimilar surfaces. Then, the matrix structure would be non-degenerative in m causing finer structures in a spectral plot of C_ν as observed in atomic spectroscopy. Thus, specific locations of the finer natural modes in ω-domain can detect all required information about the interior of the drop for in-vivo diagnostics.

FIG. 6: Mode deformability at outer (top, Fig.6a) and inner (bottom, Fig.6b) interfaces vs. acoustic excitation frequency for $l=2$ (thick lines) or $l=3$ (thin lines) where bubble-to-drop volume fraction is 0.1 (dashed), 0.3 (dash-dot) and 0.5(solid).

In Fig.6, ζ_l^{ex} and ζ_l^{in} are presented as functions of non-dimensional excitation frequency $\tilde\Omega$ for three geometries and two harmonic modes. For each case, magnitudes of both quantities approach to infinity twice in the plot when $\tilde\Omega$ coincides with either $\tilde\omega_l^+$ or $\tilde\omega_l^-$. In presence of finite viscous damping, the mode deformabilities would reach to finite maximum values under resonating conditions instead of aproaching infinity. Such characterisitics will be quantified in our future work.

V.   SUMMARY AND CONCLUDING REMARKS

There are three key results of this study. Firstly, the shifts in natural frequencies due to presence of an embedded bubble are quantified. Then, deformation amplitudes for forced vibration are estimated. Finally and most importantly, we find extra natural frequencies termed as plus mode. The last findings can help in detection of voids inside opaque droplets if its radial deformation s^{ex} at outer surface is recorded as a series of two-dimensional pictures taken in subsequent time intervals. Such data provides s^{ex} as function of time and cylindrical angle β at the viewing plane. Accordingly, a dual Fourier transform $C_\nu(\omega)$ is defined as

[1] J. Rayleigh, Proc. R. Soc. Lond. **29**, 71 (1879).
[2] R. Durisen *et al.*, Astrophys. J. **305**, 281 (1986).
[3] A. Amsden *et al.*, Phys. Rev. Lett. **35**, 905 (1975).
[4] S. Chandrasekhar, Proc. Lond. Math. Soc. **9**, 141 (1959).
[5] A. Prosperetti, J. Fluid Mech. **100**, 333 (1980).
[6] T. Lundgren and N. Mansour, J. Fluid Mech. **194**, 479 (1988).
[7] E. H. Trinh, P. L. Marston, and J. Robey, J. Colloid Interface Sci. **124**, 95 (1988).
[8] O. Basaran, J. Fluid Mech. **241**, 169 (1992).
[9] R. Apfel *et al.*, Phys. Rev. Lett. **78**, 1912 (1997).
[10] J. F. Patzer and G. M. Homsy, J. Colloids Int. Sci. **51**, 499 (1975).
[11] S. Kawano, A. Shirai, and S. Nagasaka, Phys. Fluids **19**, ARTN:012105 (2007).
[12] J. Tsamopoulos and R. Brown, J. Fluid Mech. **127**, 519

(1983).

[13] N. Pelekasis, J. Tsamopoulos, and G. Manolis, J. Fluid Mech. **230**, 541 (1991).

[14] K. A. Landman, AIChE J. **31**, 567 (1985).

[15] E. Zepper *et al.*, Phys. Rev. X Submitted (2015).

[16] M. Schwabe *et al.*, Phys. Rev. Lett. **102**, 255005 (2009).

[17] P. Yunker *et al.*, Nature **476**, 308 (2011).

[18] A. Pelosi and A. Gany, J. Propulsion and Power **28**, 1379 (2012).

[19] H. Minemawari *et al.*, Nature **475**, 364 (2011).

[20] D. Taller, D. Go, and H. Chang, Phys. Rev. Lett. **109**, 224301 (2012).

[21] V. Iyer, J. Abraham, and V. Magi, Int. J. Heat Mass Transfer **45**, 519 (2002).

[22] L. Crum and R. Roy, Science **266**, 233 (1994).

[23] T. Tszeng, J. Vibration Acoustics — Trans ASME **135**, 064504 (2013).

[24] A. Mallock, Proc. R. Soc. London, Ser. A **84**, 391 (1910).

[25] J. McDaniel, I. Akhatov, and R. Holt, Phys. Fluids **14**, 1886 (2002).

[26] X. Noblin, A. Buguin, and F. Brochard-Wyart, Phys. Rev. Lett. **94**, 166102 (2005).

[27] S. Bhattacharya, J. Chem. Phys. **128**, ARTN: 074709 (2008).

[28] S. Bhattacharya, C. Mishra, and S. Bhattacharya, J. Fluid Mech. **642**, 295 (2010).

[29] S. Navardi and S. Bhattacharya, Phys. Fluid **22**, ARTN.103306 (2010).

[30] S. Navardi and S. Bhattacharya, J. Chem. Phys. **132**, ARTN:114114 (2010).